Matrix Pencil-Based Analysis of Multirate Simulation Schemes

Liya Huang[a], Georgios Tzounas[a*]

School of Electrical and Electronic Engineering, University College Dublin, Ireland

*Corresponding author.

E-mail address: georgios.tzounas@ucd.ie

Abstract This paper focuses on multirate time-domain simulations of power system models. It proposes a matrix pencil-based approach to evaluate the spurious numerical deformation introduced into power system dynamics by a given multirate integration scheme. Moreover, it considers the problem of multirate partitioning and discusses a strategy for allocating state and algebraic variables to fast and slow subsystems based on modal participation factors (PFs). The suitability and features of the proposed approach are illustrated through numerical simulations that assess the accuracy effects of interfacing, as well as various prediction and solution methods.

Keywords: Multirate simulation, matrix pencils, numerical stability, accuracy, partitioning.

1 Introduction

1.1 Motivation

Power system dynamics are complex and span multiple timescales. This is reflected in the system model, where various components have different time constants, with some exhibiting faster and others slower responses, resulting in a set of stiff nonlinear differential algebraic equations (DAEs). Efficient and accurate time-domain simulation (TDS) of such a model is a challenging task. This paper focuses on the accuracy and numerical stability analysis of multirate methods, a family of numerical techniques that has been discussed in the literature as a means of enhancing power system TDS [1–4].

1.2 Literature Review

Multirate methods divide system variables across different timescales, simulating each with a corresponding time step size. The idea is to improve efficiency by using larger step sizes for slowly varying components, and smaller ones to accurately capture fast-changing dynamics [5–7]. Effective implementation requires addressing two key aspects [1,2,8]: partitioning system variables into different timescales; and selecting a numerical scheme to solve the equations and handle the interfacing between partitions.

Multirate partitioning can be performed once, prior to the simulation (statically) [1, 4]; or adaptively updated during the simulation (dynamically) based on the activity of variables and metrics such as local truncation errors (LTEs) [3, 9]. Dynamic partitioning promises greater accuracy, but is also more complex to implement, while its need for continuous monitoring and frequent updates of partition

boundaries increases computational cost [10]. Moreover, an important consideration for both static and dynamic partitioning is how to define the timescales of algebraic variables, as these inherently represent *infinitely fast* or *infinitely slow* dynamics. In general, there is a lack of systematic strategies to address this issue and existing approaches are heuristic. For instance, we cite [3] wherein algebraic variables are partitioned based on the rates at which algebraic equations converge during Newton's iterations. Moreover, a technique to study the link of fast/slow system dynamics with algebraic variables through the definition of appropriate *mode-in-output* PFs is presented in [11]; however, its application to multirate DAE partitioning remains unexplored. Finally, apart from the problem of multirate integration within a single simulation framework, partitioning is also crucial in multirate co-simulation, where different subsystems – such as electromagnetic transient and electromechanical models – are coupled, often across different software. In such cases, partitioning is typically performed empirically based on the natural decomposition of power system components [12–14].

Once partitioned, the power system model is numerically solved using a multirate integration scheme, where fast dynamics depend on the accurate prediction and interpolation of slow variables to maintain consistent coupling and synchronization [15]. Interfacing between fast and slow components is a particularly challenging issue: inaccurate interpolation can degrade accuracy, while the use of an explicit predictor may require smaller time steps to avoid numerical instabilities. On the other hand, implicit predictors have better stability properties but require matrix factorizations. These challenges can ultimately compromise efficiency, thus undermining the initial appeal of using a multirate method. Notably, a systematic approach to assess the accuracy and numerical stability of multirate schemes is currently missing. In this vein, recent works propose a small-signal stability analysis (SSSA) framework to evaluate the stability and accuracy of integration methods, see [16–19], but this has not yet been formulated for or applied to multirate methods.

1.3 Contribution

The contribution of the paper is twofold, as follows.

- A matrix pencil-based approach to evaluate in a unified manner the numerical stability and accuracy of multirate TDS schemes.
- A discussion on how to partition the algebraic variables of power system DAEs for multirate simulation based on mode-in-output PFs.

1.4 Paper Organization

The remainder of the paper is organized as follows. Section 2 provides preliminaries on power system multirate simulation and discusses how the variables can be partitioned into different timescales using

PFs. The proposed approach to study the numerical stability and accuracy of multirate methods is presented in Section 3. The case study is discussed in Section 4. Conclusions are drawn in Section 5.

2 Power System Multirate Simulation

2.1 DAE System Model

The short-term stability of a power system is conventionally studied through a DAE model, as follows [20]:

$$\begin{aligned} \boldsymbol{x}' &= \boldsymbol{f}(\boldsymbol{x}, \boldsymbol{y}) \\ \mathbf{0}_{m,1} &= \boldsymbol{g}(\boldsymbol{x}, \boldsymbol{y}) \end{aligned} \tag{1}$$

where $\boldsymbol{x} = \boldsymbol{x}(t) \in \mathbb{R}^n$ and $\boldsymbol{y} = \boldsymbol{y}(t) \in \mathbb{R}^m$ are the state and algebraic variables of the system, respectively; $\boldsymbol{f} : \mathbb{R}^{n+m} \mapsto \mathbb{R}^n$ and $\boldsymbol{g} : \mathbb{R}^{n+m} \mapsto \mathbb{R}^m$; $\mathbf{0}_{m,1}$ denotes the zero matrix of dimensions $m \times 1$.

A multirate simulation consists in numerically solving (1) by using different time step sizes for variables evolving in different timescales. Considering the most common case where the system is partitioned in two timescales, i.e., fast and slow, (1) can be rewritten as:

$$\boldsymbol{x}'_{\mathrm{f}} = \boldsymbol{f}_{\mathrm{f}}(\boldsymbol{x}_{\mathrm{f}}, \boldsymbol{x}_{\mathrm{s}}, \boldsymbol{y}_{\mathrm{f}}, \boldsymbol{y}_{\mathrm{s}}) \tag{2}$$

$$\mathbf{0}_{m_{\mathrm{f}},1} = \boldsymbol{g}_{\mathrm{f}}(\boldsymbol{x}_{\mathrm{f}}, \boldsymbol{x}_{\mathrm{s}}, \boldsymbol{y}_{\mathrm{f}}, \boldsymbol{y}_{\mathrm{s}}) \tag{3}$$

$$\boldsymbol{x}'_{\mathrm{s}} = \boldsymbol{f}_{\mathrm{s}}(\boldsymbol{x}_{\mathrm{f}}, \boldsymbol{x}_{\mathrm{s}}, \boldsymbol{y}_{\mathrm{f}}, \boldsymbol{y}_{\mathrm{s}}) \tag{4}$$

$$\mathbf{0}_{m_{\mathrm{s}},1} = \boldsymbol{g}_{\mathrm{s}}(\boldsymbol{x}_{\mathrm{f}}, \boldsymbol{x}_{\mathrm{s}}, \boldsymbol{y}_{\mathrm{f}}, \boldsymbol{y}_{\mathrm{s}}) \tag{5}$$

where $\boldsymbol{x}_{\mathrm{f}} \in \mathbb{R}^{n_{\mathrm{f}}}$ and $\boldsymbol{y}_{\mathrm{f}} \in \mathbb{R}^{m_{\mathrm{f}}}$ are the state and algebraic variables of the fast partition; $\boldsymbol{x}_{\mathrm{s}} \in \mathbb{R}^{n_{\mathrm{s}}}$ and $\boldsymbol{y}_{\mathrm{s}} \in \mathbb{R}^{m_{\mathrm{s}}}$ are the state and algebraic variables of the slow partition; it is $n_{\mathrm{f}} + n_{\mathrm{s}} = n$ and $m_{\mathrm{f}} + m_{\mathrm{s}} = m$.

2.2 Multirate Numerical Integration

In this section, we describe a generic multirate integration scheme employed for the solution of (2)-(5). Given the model in (2)-(5), we start from $t = t_0$, and fast and slow variables are updated with time steps h_{f} and h_{s}, respectively, where $h_{\mathrm{s}} > h_{\mathrm{f}}$. The steps of the multirate scheme, a high-level representation of which is given in Fig. 1, are as follows.

1. Predict the values of $\boldsymbol{x}$ and $\boldsymbol{y}$ at time $t + h_{\mathrm{s}}$:

$$\begin{aligned} \boldsymbol{x}^P_{t+h_{\mathrm{s}}} &= \boldsymbol{\phi}\left(\boldsymbol{x}_t, \boldsymbol{y}_t, \boldsymbol{x}_{t+h_{\mathrm{f}}}, \boldsymbol{y}_{t+h_{\mathrm{f}}}, \ldots\right) \\ \mathbf{0}_{m,1} &= h_{\mathrm{s}}\, \boldsymbol{g}\left(\boldsymbol{x}^P_{t+h_{\mathrm{s}}}, \boldsymbol{y}^P_{t+h_{\mathrm{s}}}\right) \end{aligned} \tag{6}$$

where ^{P} denotes predicted values; and $\boldsymbol{\phi} \in \mathbb{R}^n$ is defined by the predictor method adopted.

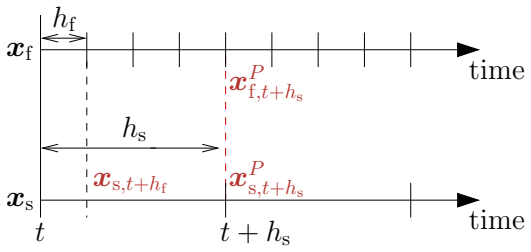

Figure 1: Representation of multirate TDS.

2. Use the predicted values to interpolate the slow variables at intermediate steps $t+ih_\mathrm{f}$, $i=1,\ldots,r$. For a generic interpolation method:

$$\begin{aligned}\boldsymbol{x}_{\mathrm{s},t+ih_\mathrm{f}} &= \boldsymbol{\imath}_\mathrm{s}(\boldsymbol{x}^P_{\mathrm{s},t+h_\mathrm{s}}, \boldsymbol{x}_{\mathrm{s},t}, r)\\ \boldsymbol{y}_{\mathrm{s},t+ih_\mathrm{f}} &= \boldsymbol{\imath}_\mathrm{s}(\boldsymbol{y}^P_{\mathrm{s},t+h_\mathrm{s}}, \boldsymbol{y}_{\mathrm{s},t}, r)\end{aligned} \tag{7}$$

where $\boldsymbol{\imath}_\mathrm{s} \in \mathbb{R}^{n_\mathrm{s}}$; and $r = h_\mathrm{s}/h_\mathrm{f} \in \mathbb{N}$.

3. Integrate the fast equations (2)-(3) with time step h_f to calculate the fast variables $\boldsymbol{x}_{\mathrm{f},t+ih_\mathrm{f}}$, $\boldsymbol{y}_{\mathrm{f},t+ih_\mathrm{f}}$ at intermediate steps $t+ih_\mathrm{f}$, $i=1,\ldots,r$.

4. Integrate the slow equations (4)-(5) at $t+h_\mathrm{s}$ with time step h_s, using the fast variables $\boldsymbol{x}_{\mathrm{f},t+rh_\mathrm{f}}$, $\boldsymbol{y}_{\mathrm{f},t+rh_\mathrm{f}}$ as inputs.

5. Compare the calculated values of the variables during the integration process with the predicted values. If $\left|\left|\boldsymbol{x}^P_{\mathrm{s},t+h_\mathrm{s}} - \boldsymbol{x}_{\mathrm{s},t+h_\mathrm{s}}\right|\right|_\infty > \varepsilon$ or $\left|\left|\boldsymbol{y}^P_{\mathrm{s},t+h_\mathrm{s}} - \boldsymbol{y}_{\mathrm{s},t+h_\mathrm{s}}\right|\right|_\infty > \varepsilon$, then update the predicted values, i.e., $\boldsymbol{x}^P_{\mathrm{s},t+h_\mathrm{s}} = \boldsymbol{x}_{\mathrm{s},t+h_\mathrm{s}}$ and $\boldsymbol{y}^P_{\mathrm{s},t+h_\mathrm{s}} = \boldsymbol{y}_{\mathrm{s},t+h_\mathrm{s}}$, and return to step 2). Otherwise, set $t = t_0 + h_\mathrm{s}$ and return to step 1).

In this paper, we consider that the predictor in step 1) may be either explicit or implicit. For steps 3) and 4) we assume that the integration method employed is implicit. As a consequence, the update of variables requires employing an iterative method. For instance, the j-th iteration of Newton's method employed for the update of fast variables in step 3) is:

$$\mathbf{J}_\mathrm{f} \begin{bmatrix}\Delta\boldsymbol{x}^{(j)}_{\mathrm{f},t+ih_\mathrm{f}}\\ \Delta\boldsymbol{y}^{(j)}_{\mathrm{f},t+ih_\mathrm{f}}\end{bmatrix} = - \begin{bmatrix}\boldsymbol{F}^{(j)}_\mathrm{f}\\ \boldsymbol{G}^{(j)}_\mathrm{f}\end{bmatrix} \tag{8}$$

where $\mathbf{J}_\mathrm{f} : \mathbb{R}^{(n_\mathrm{f}+m_\mathrm{f})\times(n_\mathrm{f}+m_\mathrm{f})}$ is the Jacobian matrix for the fast subsystem, $\boldsymbol{F}_\mathrm{f} : \mathbb{R}^{n_\mathrm{f}}$ and $\boldsymbol{G}_\mathrm{f} : \mathbb{R}^{m_\mathrm{f}}$ are defined by the implicit integration method adopted. To speed up the solution, a dishonest Newton (DHN) method can be used, wherein $\mathbf{J}_\mathrm{f}$ is factorized only once per time step. Using DHN in the process above, a summary of the Jacobian factorizations required per time increment h_s for different integration schemes is given in Table 1. We note that a complete assessment of computational efficiency

should be based on performance indicators (e.g., wall-clock time). Moreover, meaningful comparisons between different multirate setups require adjusting the time step sizes for each configuration to achieve comparable numerical accuracy. The matrix-pencil-based approach presented in Section 3 can be used to select such step sizes.

Table 1: Number of Jacobian factorizations every h_s using DHN: Single-rate, multirate with explicit predictor, and multirate with implicit predictor.

	Matrix order			
Multirate	$n+m$	m_s	$n_\mathrm{f}+m_\mathrm{f}$	$n_\mathrm{s}+m_\mathrm{s}$
No, step h_f	r	0	0	0
Yes, explicit predictor	0	1	r	1
Yes, implicit predictor	1	0	r	1

2.3 PF-Based Partitioning

This section focuses on how to define (2)-(5) given (1), i.e., on the partitioning of system variables into fast and slow subsets. As discussed in Section 1, algebraic variables do not define any dynamics of finite speed and are thus more challenging to partition than states.

To address this issue, [3] proposes to evaluate the speed of algebraic variables dynamically, based on the number of Newton iterations required for their equations to converge during the simulation. Variables that converge in a small number of iterations are classified as fast, whereas those requiring more iterations are considered slow. Although this approach may be accurate in some cases, it also has significant limitations. For example, consider an infinitely slow algebraic variable y defined through the equation $0 = y - y_o$, where y_o is a constant.[1] The equation converges trivially in a single iteration and y is thus misclassified as fast by the above approach, despite being infinitely slow.

In this paper, we avoid characterizing the speeds of variables – which is a property of the model – through purely numerical indicators. Instead, we adopt a principled partitioning strategy, based on matrix pencil-based SSSA and PFs. Linearization of (1) at an equilibrium $(\boldsymbol{x}_o, \boldsymbol{y}_o) := [\boldsymbol{x}_o^\intercal \ \boldsymbol{y}_o^\intercal]^\intercal$ gives:

$$\begin{aligned} \widetilde{\boldsymbol{x}}' &= \boldsymbol{f}_x \widetilde{\boldsymbol{x}} + \boldsymbol{f}_y \widetilde{\boldsymbol{y}} \\ \boldsymbol{0}_{m,1} &= \boldsymbol{g}_x \widetilde{\boldsymbol{x}} + \boldsymbol{g}_y \widetilde{\boldsymbol{y}} \end{aligned} \tag{9}$$

where $\widetilde{\boldsymbol{x}} = \boldsymbol{x} - \boldsymbol{x}_0$, $\widetilde{\boldsymbol{y}} = \boldsymbol{y} - \boldsymbol{y}_0$; and $\boldsymbol{f}_x$, $\boldsymbol{f}_y$, $\boldsymbol{g}_x$, $\boldsymbol{g}_y$ are Jacobian matrices at $(\boldsymbol{x}_0, \boldsymbol{y}_0)$ (where $^\intercal$ is the matrix transpose). System (9) can be rewritten as:

$$\mathbf{E}\,\mathbf{x}' = \mathbf{A}\,\mathbf{x} \tag{10}$$

[1] y is infinitely slow as $y' = 0$, or, $Ty' = g(y)$ with $T \to \infty$. Relevant examples in a power system model include, e.g. auxiliary control variables that define fixed setpoints.

where $\mathbf{x} = (\widetilde{\boldsymbol{x}}, \widetilde{\boldsymbol{y}})$; $\boldsymbol{I}_n$ is the $n \times n$ identity matrix; and:

$$\mathbf{E} = \begin{bmatrix} \boldsymbol{I}_n & \mathbf{0}_{n,m} \\ \mathbf{0}_{m,n} & \mathbf{0}_m \end{bmatrix}, \quad \mathbf{A} = \begin{bmatrix} \boldsymbol{f}_x & \boldsymbol{f}_y \\ \boldsymbol{g}_x & \boldsymbol{g}_y \end{bmatrix} \tag{11}$$

where $\mathbf{0}_m$ is the zero matrix of dimensions $m \times m$. The algebraic variables can be eliminated under the assumption that the Jacobian matrix $\boldsymbol{g}_y$ is invertible. This assumption comes with no loss of generality, as potential singularities can be always resolved by reformulating the DAE system into a dynamically equivalent form with a non-singular $\boldsymbol{g}_y$ [21]. The elimination yields:

$$\widetilde{\boldsymbol{x}}' = \boldsymbol{\mathcal{A}}\, \widetilde{\boldsymbol{x}} \tag{12}$$

where $\boldsymbol{\mathcal{A}} = \boldsymbol{f}_x - \boldsymbol{f}_y \boldsymbol{g}_y^{-1} \boldsymbol{g}_x$. The eigenvalues of $\boldsymbol{\mathcal{A}}$ are then found by solving the algebraic problem [22]:

$$\begin{aligned} (s\boldsymbol{I}_n - \boldsymbol{\mathcal{A}})\, \boldsymbol{v} &= \mathbf{0}_{n,1} \\ \boldsymbol{w}\, (s\boldsymbol{I}_n - \boldsymbol{\mathcal{A}}) &= \mathbf{0}_{1,n} \end{aligned} \tag{13}$$

Every $s \in \mathbb{C}$ satisfying (13) is an eigenvalue of $\boldsymbol{\mathcal{A}}$, with $\boldsymbol{v}$ and $\boldsymbol{w}$ being the corresponding right and left eigenvectors. Moreover, the right and left modal matrices (12) are $\boldsymbol{V} = [\boldsymbol{v}_1 \cdots \boldsymbol{v}_n]$ and $\boldsymbol{W} = [\boldsymbol{w}_1^\intercal \cdots \boldsymbol{w}_n^\intercal]^\intercal$. Provided that the eigenvalues of $\boldsymbol{\mathcal{A}}$ have equal algebraic and geometric multiplicities, the evolution of the k-th element of $\widetilde{\boldsymbol{x}}$ is:

$$\widetilde{x}_k(t) = \sum_{i=1}^{n} e^{s_i t} \boldsymbol{w}_i \widetilde{\boldsymbol{x}}(0) v_{k,i} \tag{14}$$

where $v_{k,i}$, $w_{i,k}$ are the k-th elements of $\boldsymbol{v}_i$, $\boldsymbol{w}_i$, respectively. Exciting in the k-th differential equation the k-th state, e.g., by applying the initial conditions $\widetilde{x}_k(0) = 1$, and $\widetilde{x}_h(0) = 0$, $h \neq k$, we get:

$$\widetilde{x}_k(t) = \sum_{i=1}^{n} w_{i,k} v_{k,i} e^{s_i t} = \sum_{i=1}^{n} p_{ki}^{[x]} e^{s_i t} \tag{15}$$

where $p_{ki}^{[x]} = w_{i,k} v_{k,i}$ is called mode-in-state PF and provides a measure of the contribution of the i-th eigenvalue s_i to the k-th state variation $\widetilde{x}_k$. Then, the system's state participation matrix $\mathbf{P}_x \in \mathbb{R}^{n \times n}$ is defined as:

$$\mathbf{P}_x = (p_{ki}^{[x]})_{1 \leq (k,i) \leq n} = \boldsymbol{W}^\intercal \circ \boldsymbol{V} \tag{16}$$

where $\circ$ denotes the Hadamard product. Given $\mathbf{P}_x$, the participation matrix of algebraic variables $\mathbf{P}_y \in \mathbb{R}^{m \times n}$ is defined as [11]:

$$\mathbf{P}_y = -\boldsymbol{g}_y^{-1} \boldsymbol{g}_x \mathbf{P}_x \tag{17}$$

The derivation of (17) is provided in Appendix A. To ensure that PFs of different algebraic variables are comparable, each row of $\mathbf{P}_y$ is normalized by dividing with the Euclidean norm of its entries [23].

In this paper, state and algebraic variables are partitioned into fast and slow subsets by using the participation matrices $\mathbf{P}_x$ and $\mathbf{P}_y$. In particular, by comparing the absolute values of the elements in each row of $\mathbf{P}_x$, we identify the eigenvalue that has the largest contribution to each state variable of the system, and denote it as $\lambda_{x,k}$ $(k = 1, 2, \ldots, n)$. Similarly, by comparing the absolute values of the elements in each row of $\mathbf{P}_y$, we identify the eigenvalue that has the largest contribution to each algebraic variable, and denote it as $\lambda_{y,j}$ $(j = 1, 2, \ldots, m)$. Then, based on the natural frequencies of $\lambda_{x,k}$ and $\lambda_{y,j}$, state and algebraic variables are partitioned with a timescale separation natural angular frequency threshold δ. For example, an algebraic variable is considered fast if $|\lambda_{y,j}| > \delta$; otherwise, it is slow.

3 Numerical Stability and Accuracy

3.1 Formulation

In this section, we present a matrix pencil-based approach to analyze the numerical stability and precision of multirate integration methods. The main idea is that the spurious numerical deformation introduced to the dynamics of (1) by a given multirate scheme can be quantified by studying a linear discrete-time system of the following form:

$$\mathbf{F}_r \, \mathbf{y}_{t+h_s} = \mathbf{G}_r \, \mathbf{y}_t \tag{18}$$

where $\mathbf{F}_r$, $\mathbf{G}_r$ and $\mathbf{y}_t$ are defined from the specific multirate scheme implemented. Specifically, (18) represents the small-signal dynamics of (1) as approximated by the multirate scheme. The approximated dynamics, in turn, depend on how the system is partitioned, i.e., on how (2)-(5) are defined; as well as on the numerical scheme chosen for the solution of the system, i.e., on the specific implementation of steps 1)-5) in Section 2.2. The stability of (18) can be seen through the properties of the z-domain matrix pencil $\widehat{z}\mathbf{F}_r - \mathbf{G}_r$, where $\widehat{z} \in \mathbb{C}$. In particular, (18) is asymptotically stable if for every eigenvalue $\widehat{z}_i$ of $\widehat{z}\mathbf{F}_r - \mathbf{G}_r$, it holds that $|\widehat{z}_i| < 1$. An instability of (18) indicates numerical instability of the multirate scheme. Moreover, the numerical deformation introduced to the dynamic modes of the power system model by the multirate method can be seen by comparing the eigenvalues of $\widehat{z}\mathbf{F}_r - \mathbf{G}_r$ to those of $s\boldsymbol{I}_n - \boldsymbol{\mathcal{A}}$. For a given eigenvalue s_i of $s\boldsymbol{I}_n - \boldsymbol{\mathcal{A}}$, the relative deformation is $|\widehat{s}_i - s_i|/|s_i|$ where $\widehat{s}_i = \log(\widehat{z}_i)/h_\mathrm{f}$ is the corresponding numerically deformed eigenvalue, mapped to the s-domain to facilitate comparison.

3.2 Application to Illustrative Multirate Scheme

In this section, we illustrate the proposed matrix pencil-based numerical stability and accuracy analysis. To this end, we consider an implementation of steps 1)-5) in Subsection 2.2 that presents similarities

with the scheme adopted in [3]. In particular, we consider prediction in step 1) by the forward Euler method (FEM), and solution of fast and slow variables in steps 3) and 4 by the trapezoidal method (TM). The process at the time interval $[t_0, t + h_\mathrm{s}]$ is described as follows.

In step 1), the values of all variables are predicted using FEM:

$$\begin{aligned} \boldsymbol{x}^P_{t+h_\mathrm{s}} &= \boldsymbol{x}_t + h_\mathrm{s}\boldsymbol{f}(\boldsymbol{x}_t, \boldsymbol{y}_t) \\ \mathbf{0}_{m,1} &= h_\mathrm{s}\boldsymbol{g}(\boldsymbol{x}^P_{t+h_\mathrm{s}}, \boldsymbol{y}^P_{t+h_\mathrm{s}}) \end{aligned} \tag{19}$$

In step 2), the values of the slow variables at intermediate steps $t + ih_\mathrm{f}$ are interpolated linearly:

$$\begin{aligned} \boldsymbol{x}_{\mathrm{s},t+ih_\mathrm{f}} &= i(\boldsymbol{x}^P_{\mathrm{s},t+h_\mathrm{s}} - \boldsymbol{x}_{\mathrm{s},t})/r + \boldsymbol{x}_{\mathrm{s},t} \\ \boldsymbol{y}_{\mathrm{s},t+ih_\mathrm{f}} &= i(\boldsymbol{y}^P_{\mathrm{s},t+h_\mathrm{s}} - \boldsymbol{y}_{\mathrm{s},t})/r + \boldsymbol{y}_{\mathrm{s},t} \end{aligned} \tag{20}$$

In step 3), fast equations at $t+ih_\mathrm{f}$ are solved with TM:

$$\begin{aligned} \boldsymbol{x}_{\mathrm{f},t+ih_\mathrm{f}} =& \boldsymbol{x}_{\mathrm{f},t+(i-1)h_\mathrm{f}} + \frac{h_\mathrm{f}}{2}\boldsymbol{f}_\mathrm{f}(\boldsymbol{x}_{t+ih_\mathrm{f}}, \boldsymbol{y}_{t+ih_\mathrm{f}}) \\ &+ \frac{h_\mathrm{f}}{2}\boldsymbol{f}_\mathrm{f}(\boldsymbol{x}_{t+(i-1)h_\mathrm{f}}, \boldsymbol{y}_{t+(i-1)h_\mathrm{f}}) \\ \mathbf{0}_{m_\mathrm{f},1} =& h_\mathrm{f}\boldsymbol{g}_\mathrm{f}(\boldsymbol{x}_{t+ih_\mathrm{f}}, \boldsymbol{y}_{t+ih_\mathrm{f}}) \end{aligned} \tag{21}$$

In step 4), slow equations at $t+h_\mathrm{s}$ are solved with TM:

$$\begin{aligned} \boldsymbol{x}_{\mathrm{s},t+h_\mathrm{s}} &= \boldsymbol{x}_{\mathrm{s},t} + \frac{h_\mathrm{s}}{2}\boldsymbol{f}_\mathrm{s}(\boldsymbol{x}_t, \boldsymbol{y}_t) + \frac{h_\mathrm{s}}{2}\boldsymbol{f}_\mathrm{s}(\boldsymbol{x}_{t+h_\mathrm{s}}, \boldsymbol{y}_{t+h_\mathrm{s}}) \\ \mathbf{0}_{m_\mathrm{s},1} &= h_\mathrm{s}\boldsymbol{g}_\mathrm{s}(\boldsymbol{x}_{t+h_\mathrm{s}}, \boldsymbol{y}_{t+h_\mathrm{s}}) \end{aligned} \tag{22}$$

We proceed to apply the proposed analysis as described in Section 3.1. To this end, we linearize (19)-(22) around the equilibrium $(\boldsymbol{x}_o, \boldsymbol{y}_o)$, which is also a fixed point of (19)-(22) under the assumption that $(\boldsymbol{x}_{t+\tau}, \boldsymbol{y}_{t+\tau}) = (\boldsymbol{x}_o, \boldsymbol{y}_o)$ for $\tau \in [-h_\mathrm{s}, 0]$.

Linearization of (19) gives:

$$\begin{aligned} \widetilde{\boldsymbol{x}}^P_{t+h_\mathrm{s}} &= \widetilde{\boldsymbol{x}}_t + h_\mathrm{s}\left(\boldsymbol{f}_x\widetilde{\boldsymbol{x}}_t + \boldsymbol{f}_y\widetilde{\boldsymbol{y}}_t\right) \\ \mathbf{0}_{m,1} &= \boldsymbol{g}_x\widetilde{\boldsymbol{x}}^P_{t+h_\mathrm{s}} + \boldsymbol{g}_y\widetilde{\boldsymbol{y}}^P_{t+h_\mathrm{s}} \end{aligned} \tag{23}$$

Linearization of (20) gives:

$$\begin{aligned} \widetilde{\boldsymbol{x}}_{\mathrm{s},t+h_\mathrm{f}} &= (\widetilde{\boldsymbol{x}}^P_{\mathrm{s},t+h_\mathrm{s}} - \widetilde{\boldsymbol{x}}_{\mathrm{s},t})/r + \widetilde{\boldsymbol{x}}_{\mathrm{s},t} \\ \widetilde{\boldsymbol{y}}_{\mathrm{s},t+h_\mathrm{f}} &= (\widetilde{\boldsymbol{y}}^P_{\mathrm{s},t+h_\mathrm{s}} - \widetilde{\boldsymbol{y}}_{\mathrm{s},t})/r + \widetilde{\boldsymbol{y}}_{\mathrm{s},t} \end{aligned} \tag{24}$$

Linearization of (21) gives:

$$\begin{aligned}\widetilde{\boldsymbol{x}}_{\mathrm{f},t+ih_\mathrm{f}} =&\widetilde{\boldsymbol{x}}_{\mathrm{f},t+(i-1)h_\mathrm{f}} + \frac{h_\mathrm{f}}{2}(\boldsymbol{f}_{\mathrm{f},x}\widetilde{\boldsymbol{x}}_{t+ih_\mathrm{f}} + \boldsymbol{f}_{\mathrm{f},y}\widetilde{\boldsymbol{y}}_{t+ih_\mathrm{f}}) \\ &+ \frac{h_\mathrm{f}}{2}(\boldsymbol{f}_{\mathrm{f},x}\widetilde{\boldsymbol{x}}_{t+(i-1)h_\mathrm{f}}+\boldsymbol{f}_{\mathrm{f},y}\widetilde{\boldsymbol{y}}_{t+(i-1)h_\mathrm{f}}) \\ \mathbf{0}_{m_\mathrm{f},1} =& h_\mathrm{f}\left(\boldsymbol{g}_{\mathrm{f},x}\widetilde{\boldsymbol{x}}_{t+ih_\mathrm{f}} + \boldsymbol{g}_{\mathrm{f},y}\widetilde{\boldsymbol{y}}_{t+ih_\mathrm{f}}\right)\end{aligned} \tag{25}$$

Finally, linearization of (22) gives:

$$\begin{aligned}\widetilde{\boldsymbol{x}}_{\mathrm{s},t+h_\mathrm{s}} =& \widetilde{\boldsymbol{x}}_{\mathrm{s},t} + \frac{h_\mathrm{s}}{2}(\boldsymbol{f}_{\mathrm{s},x}\widetilde{\boldsymbol{x}}_{t+h_\mathrm{s}} + \boldsymbol{f}_{\mathrm{s},y}\widetilde{\boldsymbol{y}}_{t+h_\mathrm{s}}) \\ &+ \frac{h_\mathrm{s}}{2}(\boldsymbol{f}_{\mathrm{s},x}\widetilde{\boldsymbol{x}}_{t} + \boldsymbol{f}_{\mathrm{s},y}\widetilde{\boldsymbol{y}}_{t}) \\ \mathbf{0}_{m_\mathrm{s},1} =& h_\mathrm{s}\left(\boldsymbol{g}_{\mathrm{s},x}\widetilde{\boldsymbol{x}}_{t+h_\mathrm{s}} + \boldsymbol{g}_{\mathrm{s},y}\widetilde{\boldsymbol{y}}_{t+h_\mathrm{s}}\right)\end{aligned} \tag{26}$$

We provide the following proposition.

Proposition 1: The spectral properties of (23)-(26) can be seen by studying an equivalent discrete-time system in the form of (18), where $\mathbf{y}_{t+h_\mathrm{s}} = (\mathbf{x}_{t+rh_\mathrm{f}}, \dots \mathbf{x}_{t+h_\mathrm{f}})$, $\mathbf{y}_t = (\mathbf{x}_{t+(r-1)h_\mathrm{f}}, \dots, \mathbf{x}_t)$, and $\mathbf{G}_r$, $\mathbf{F}_r$ are properly defined matrices.

The proof of Proposition 1 is provided in Appendix B and is written in a general way to accommodate a broader class of predictor and corrector methods through a parameterized representation. Then, following from this proof, the case study discussed in the next section compares the accuracy of multirate schemes implemented using different predictor and fast/slow variables solution methods.

4 Case Study

This section presents simulation results based on the well-known WSCC 9-bus benchmark system [24]. The system consists of 6 transmission lines and 3 medium voltage/high voltage transformers; 3 synchronous generators (SGs) equipped with automatic voltage regulators (AVRs), power system stabilizers (PSSs), and turbine governors (TGs). In total, the system's DAE model includes 33 state and 64 algebraic variables. Simulation results are obtained with Dome [25]. Eigenvalues are computed with LAPACK [26].

We start by partitioning the system variables using the participation matrices $\mathbf{P}_x$ and $\mathbf{P}_y$ as discussed in Section 2.3 and where we have set $\delta = 20$. As a result, the states representing the AVR voltages, along with the algebraic variables representing the SG field voltages, are allocated to the fast subsystem. For the sake of comparison, we also consider the scenario where state variables are partitioned through standard PF analysis, whereas all algebraic variables are classified as fast. Assuming the multirate scheme described in Subsection 3.2 – i.e., prediction in step 1) is made with FEM and solution of

Table 2: PF-based partitioning: relative numerical deformation of dominant mode.

h_f [s]	h_s [s]	PF-based for $\boldsymbol{x}$ and $\boldsymbol{y}$	PF-based for $\boldsymbol{x}$; ($\boldsymbol{y} = \boldsymbol{y}_\mathrm{f}$)
	0.005	0.42%	0.42%
0.001	0.01	0.42%	0.42%
	0.05	0.42%	0.42%
0.002		0.84%	0.838%
0.004	0.1	1.68%	1.68%
0.005		2.10%	2.09%

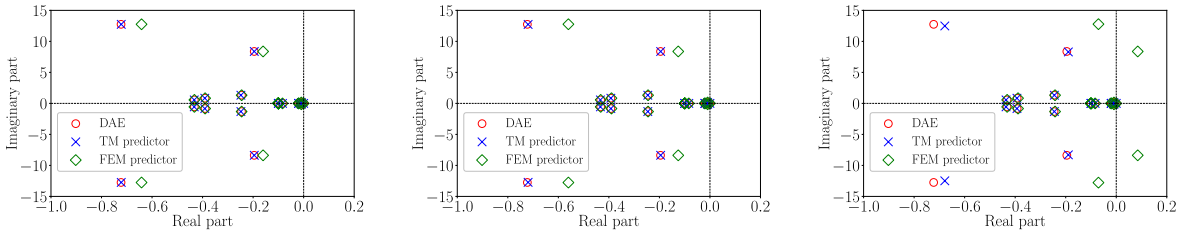

(a) $h_\mathrm{s} = 0.005$ s, $h_\mathrm{f} = 0.001$ s. (b) $h_\mathrm{s} = 0.01$ s, $h_\mathrm{f} = 0.002$ s. (c) $h_\mathrm{s} = 0.04$ s, $h_\mathrm{f} = 0.008$ s.

Figure 2: Eigenvalue analysis of multirate schemes: FEM prediction vs. TM prediction.

fast/slow variables in steps 3) and 4) is achieved with TM – a first comparison of the two partitioning strategies is provided in Table 2. In particular, the table employs the proposed matrix pencil-based approach described in Subsection 3.1 to quantify the relative numerical deformation introduced to the system's dominant dynamic mode by the two partitioning strategies. The dominant mode refers to the local electromechanical oscillation of the SG connected to bus 2. In the eigenvalue analysis, this mode is represented by the complex pair $-0.19561 \pm j8.37291$ and has damping ratio $\zeta = 2.79\%$. Table 2 suggests that a principled allocation of a subset of the algebraic variables to the slow timescale based on their PFs achieves accuracy comparable to assuming that all algebraic variables are fast ($\boldsymbol{y} = \boldsymbol{y}_\mathrm{f}$), thereby showing potential to improve simulation speed. All results in the remainder of this section are produced by considering PF-based partitioning of both state and algebraic variables.

We proceed to compare the impact of altering the multirate scheme's predictor method on the numerical deformation introduced to the system dynamic modes. The results under different time steps for prediction by FEM and TM are shown in Fig. 2. As expected, TM prediction outperforms FEM in terms of accuracy. In fact, as the time steps h_s and h_f are increased, the accuracy of FEM significantly deteriorates and eventually numerical instability is encountered. On the other hand, with TM prediction numerical stability is maintained regardless of the selected time step sizes, although this naturally comes at an additional computational cost due to the need for full Jacobian factorization in step 1).

In Fig. 3, we fix the ratio $r = h_\mathrm{s}/h_\mathrm{f}$ to 10 and study the trajectory of the dominant mode's numerical deformation over the range $h_\mathrm{f} = [0.0001, 0.005]$ s and $h_\mathrm{s} = [0.001, 0.05]$ s. To this end, we consider different implementations of steps 1), 3) and 4) in Section 3.2. In the figure, solving fast/slow variables

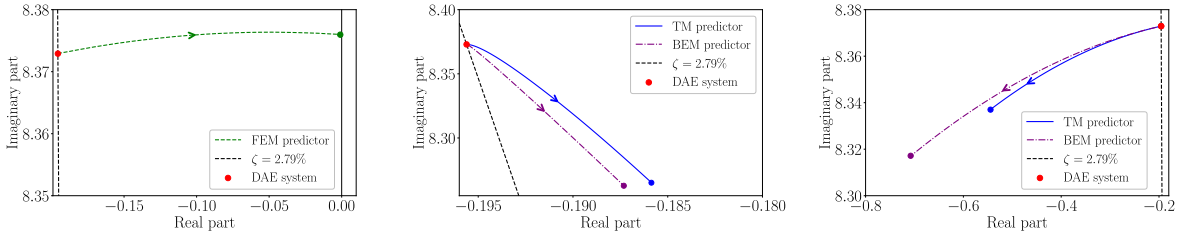

(a) FEM prediction, TM solution. (b) Implicit prediction, TM solution. (c) Implicit prediction, BEM solution.

Figure 3: Multirate integration: Dominant mode deformation as h_f increases from 10^{-4} to 0.005 s, $r = 10$. The points at the end of each line correspond to $h_\mathrm{f} = 0.005$ s.

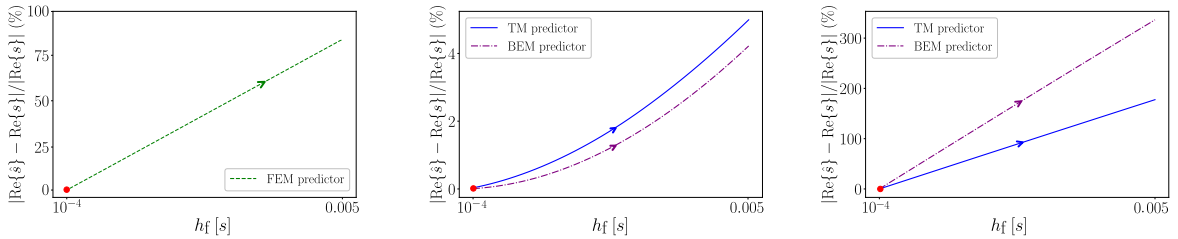

(a) FEM prediction, TM solution. (b) Implicit prediction, TM solution. (c) Implicit prediction, BEM solution.

Figure 4: Real part deformation of dominant mode as h_f increases from 10^{-4} to 0.005 s, $r = 10$.

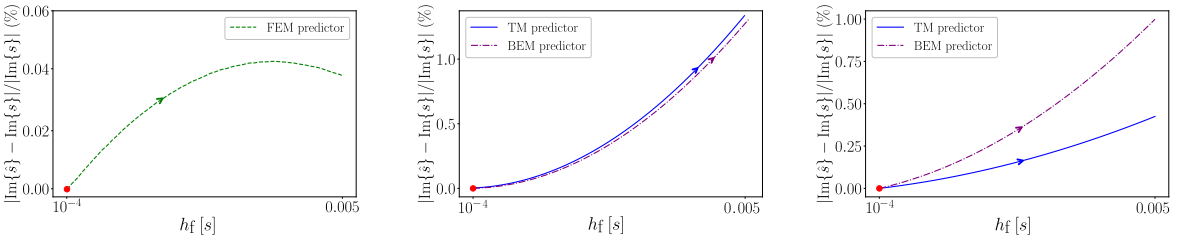

(a) FEM prediction, TM solution. (b) Implicit prediction, TM solution. (c) Implicit prediction, BEM solution.

Figure 5: Imaginary part deformation of dominant mode as h_f increases from 10^{-4} to 0.005 s, $r = 10$.

with TM in steps 3) and 4) is referred to as "TM solution". As shown in Fig. 3a, the critical value of h_f beyond which the integration scheme is guaranteed to be destabilized under FEM prediction is 0.005 s. Moreover, from Fig. 3b it can be observed that when all steps 1), 3) and 4) are implemented using TM, the multirate scheme can exhibit slight underdamping. This underdamping can be mitigated by using backward Euler method (BEM) for prediction. Yet, as expected, if all steps 1), 3) and 4) are implemented with BEM, the multirate scheme can lead to significant numerical overdamping. This is illustrated in Fig. 3c. For the same mode, the numerical deformation of the real and imaginary parts of the corresponding eigenvalue are shown in Figs. 4 and 5, respectively. Figure 5 explicitly shows the deformation in the imaginary part, capturing the spurious numerical shift in oscillation frequency. Under TM solution, prediction with TM results in slightly greater imaginary part deformation than BEM. Conversely, under BEM solution, prediction with BEM yields smaller deformation than TM. Overall, the highest level of accuracy in the examined cases is achieved when a BEM predictor is combined with TM solution of fast/slow variables.

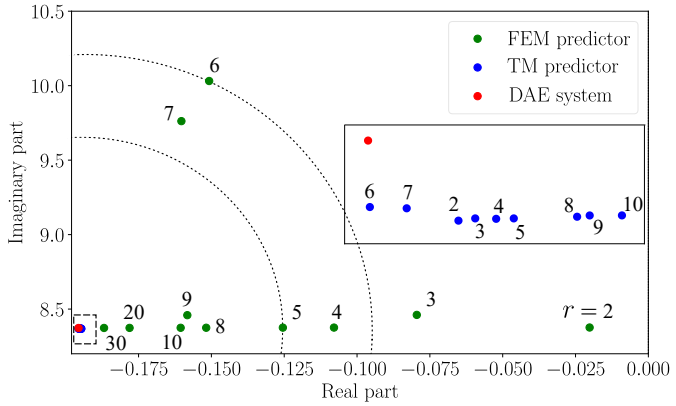

Figure 6: Dominant mode deformation with FEM and TM predictors under different time step ratios ($h_\mathrm{s} = 0.05$ s). The numbers next to the points represent the ratio values.

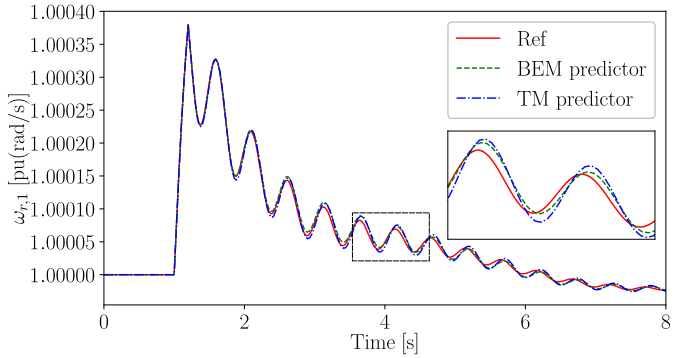

Figure 7: $\omega_{r,1}$ after the load trip at bus 5 with TM solution. $h_\mathrm{s} = 0.05$ s, $h_\mathrm{f} = 0.005$ s.

We further assess the numerical deformation of the system's dominant mode by examining the impact of varying the ratio $r = h_\mathrm{s}/h_\mathrm{f}$. To this end, we keep h_s constant and vary r by changing h_f. Fast/slow variables are solved with TM. The results are presented in Fig. 6, and indicate that, interestingly, smaller values of h_f do not necessarily imply better accuracy. For example, with FEM prediction, increasing r from 5 to 6 leads to a larger numerical deformation. Although counterintuitive at a first glance, this irregular behavior occurs as decreasing h_f increases the number of intermediate steps that rely on linearly interpolated values of the slow variables, which are not updated until $t + h_\mathrm{s}$, thus amplifying interfacing error.

In the following, we perform multirate non-linear time-domain simulations of the system's non-linear DAE model. In particular, we consider the response of the system after (i) a sudden trip of 50% of the load connected to bus 5 occurring at $t = 1$ s and followed by reconnection at $t = 1.2$ s; and (ii) a three-phase fault occurring at bus 5 at $t = 1$ s and cleared after 100 ms by tripping the line that connects buses 5 and 7. The simulation results in Fig. 7 to Fig. 10 show the response of $\omega_{\mathrm{r},1}$ following each disturbance. Four different multirate setups are considered for prediction of slow variables and solution of fast/slow variables, namely, BEM prediction with TM solution; TM prediction with TM solution; BEM prediction with BEM solution; and TM prediction with BEM solution. Reference trajectories

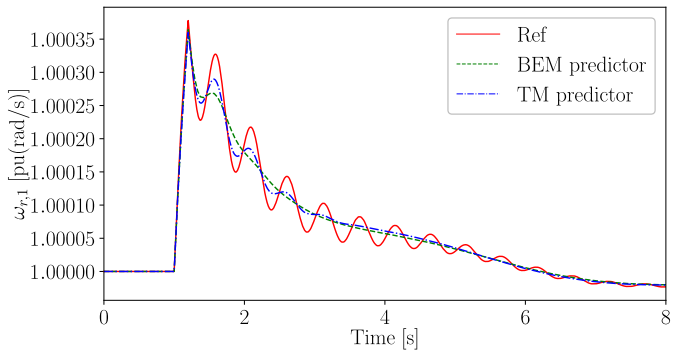

Figure 8: $\omega_{r,1}$ after the load trip at bus 5 with BEM solution. $h_{\mathrm{s}} = 0.05$ s, $h_{\mathrm{f}} = 0.005$ s.

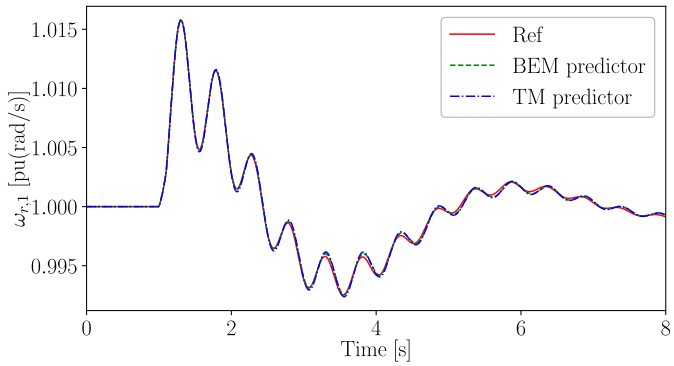

Figure 9: $\omega_{r,1}$ after the fault at bus 5 with TM solution. $h_{\mathrm{s}} = 0.05$ s, $h_{\mathrm{f}} = 0.005$ s.

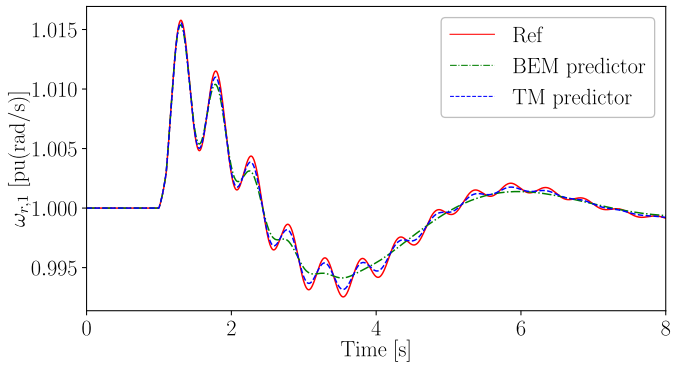

Figure 10: $\omega_{r,1}$ after the fault at bus 5 with BEM solution. $h_{\mathrm{s}} = 0.05$ s, $h_{\mathrm{f}} = 0.005$ s.

here and in the remainder of the paper are obtained using a two-stage diagonally implicit Runge-Kutta method with time step $h = 0.001$ s. From Fig. 7 and Fig. 9, it can be seen that TM solution can lead to slight underdamping, which is mitigated when coupled with BEM prediction. Moreover, from Fig. 8 and Fig. 10, it can be seen that BEM solution can result in significant numerical overdamping, which is mitigated when combined with TM predictor. The results also indicate that the multirate scheme introduces small oscillation frequency shifts. These results are consistent with the conclusions obtained from the matrix pencil-based SSSA in Figs. 3-5.

We further examine the effect of interpolation of the slow variables. Figure 11 shows the numerical

error of the trajectory of machine 1 ($\omega_{\mathrm{r},1}$) following the fault at bus 5, comparing linear and cubic spline interpolation for different time step ratios r, using TM prediction and TM solution. Figure 11a confirms the occurrence of irregular numerical deformation when linear interpolation is used (see also Fig. 6). In contrast, these irregularities are eliminated when cubic spline interpolation is applied, as shown in Fig. 11b. In all cases examined, spline interpolation yields smaller errors than linear interpolation.

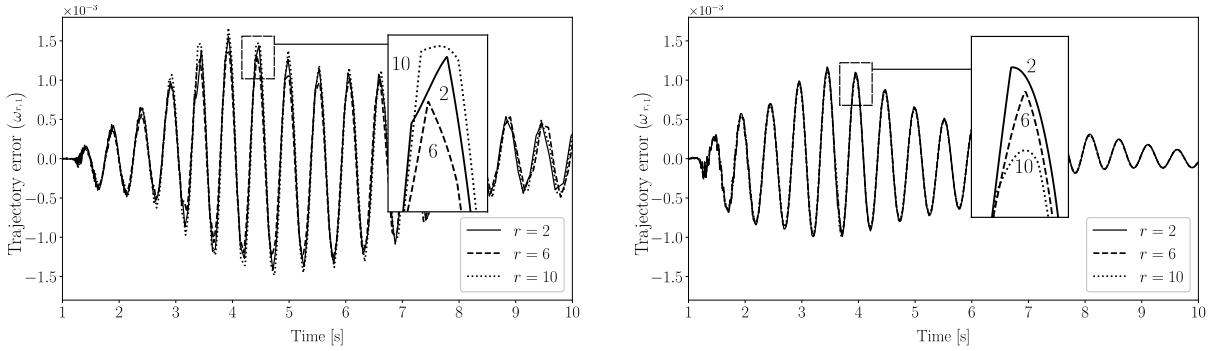

(a) Linear interpolation.

(b) Cubic spline interpolation.

Figure 11: Trajectory error of $\omega_{\mathrm{r},1}$ under fault at bus 5: linear vs. cubic spline interpolation.

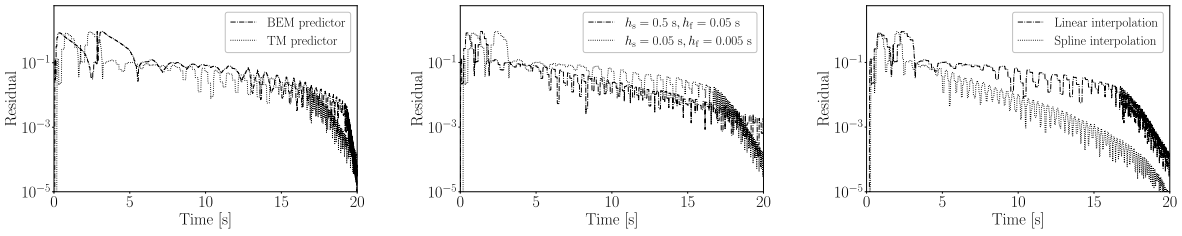

(a) Predictor: BEM vs. TM.

(b) Different time steps.

(c) Interpolation: linear vs. cubic spline.

Figure 12: Fault at bus 5, TM solution ($h_s = 0.005$ s, $h_f = 0.001$ s): algebraic residual of slow subsystem.

Another relevant issue associated with interpolation of the slow variables is the appearance of algebraic constraint residuals. As described in Section 2.2, fast variables are solved at every step, while the slow variables are updated at the slow time scale. During intermediate steps, the slow variables are not solved but interpolated, so the algebraic equations involving $\boldsymbol{y}_{\mathrm{s}}$ may indeed exhibit residuals. Figure 12 shows the evolution of the Euclidean norm of the algebraic constraint residuals of the slow subsystem. The residuals increase following the disturbance and gradually decrease as the system approaches steady-state conditions. Yet, it is worth noting that even if residuals are very small, this does not imply that the overall numerical solution is accurate.

We finally discuss the impact of varying the partitioning threshold δ on mode deformation for both the original WSCC system and a modified version with increased stiffness, where part of the synchronous generation is replaced by inverter-based resources (IBRs). As seen in Fig. 13a, for a given fast time step size, $\delta = 0$ leads to a single-rate simulation where all variables are integrated with the fast step, resulting in minimal mode deformation for this setup. As δ increases, more variables are assigned to the slow subsystem, and for a fixed h_{s}, the deformation tends to grow. We note that, in practice, varying δ would

generally affect the selection of h_{s} to provide a good trade-off between accuracy and computational cost. Figures 13b and 13c compare the error during the three-phase fault at bus 5 using TM prediction with TM solution for different values of δ; the results are consistent with those of small-signal analysis.

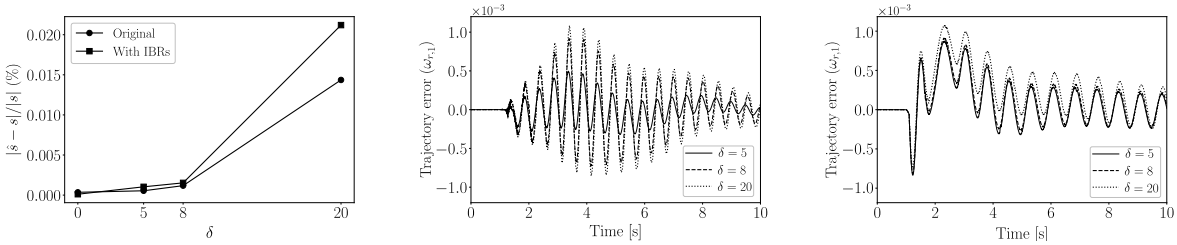

(a) Dominant mode numerical deformation. (b) Original system. (c) Modified system with IBRs.

Figure 13: Impact of changing the partitioning threshold δ ($h_s = 0.005$ s, $h_f = 0.001$ s).

5 Conclusion

The paper presents a matrix pencil-based approach for analyzing the numerical stability and accuracy of multirate time-domain simulation schemes applied to power system DAEs. By expressing the discretized small-signal multirate model as a system of linear difference equations, our approach enables the systematic assessment of spurious numerical mode deformation. In addition, a principled strategy for partitioning both state and algebraic variables based on modal participation factors is discussed. The proposed approach is used to evaluate the impact of different predictor types, integration methods, and time step sizes, revealing nontrivial accuracy trends. Our findings support the use of small-signal tools to guide the design of multirate schemes in practical applications.

Future work will explore the application of multirate methods in co-simulation frameworks for large-scale power systems involving electromagnetic transients, as well as further investigate the capabilities of PF-based partitioning strategies.

6 Funding

This work is supported by the China Scholarship Council, by funding L. Huang; and by Science Foundation Ireland, by funding G. Tzounas under project NexSys (grant. no. 21/SPP/3756).

Appendix A Derivation of (17)

By treating algebraic variables as outputs of the system's state-space with output matrix $\boldsymbol{C} \in \mathbb{R}^{m \times n}$, i.e., $\widetilde{\boldsymbol{y}} = \boldsymbol{C}\widetilde{\boldsymbol{x}}$, from the second equation in (9) we get that $\boldsymbol{C} = -\boldsymbol{g}_y^{-1}\boldsymbol{g}_x$. Denoting the μ-th row as

$\boldsymbol{C}_\mu = [c_{\mu 1}, \ldots, c_{\mu n}]$, $\widetilde{y}_\mu$ is given by:

$$\widetilde{y}_\mu = \boldsymbol{C}_\mu \widetilde{\boldsymbol{x}} = c_{\mu 1}\widetilde{x}_1 + c_{\mu 2}\widetilde{x}_2 + \cdots + c_{\mu n}\widetilde{x}_n \tag{A.1}$$

And, by using (15):

$$\widetilde{y}_\mu = \sum_{i=1}^{n}(c_{\mu 1}p_{1i}^{[x]} + \cdots + c_{\mu n}p_{ni}^{[x]})e^{s_i t} = \sum_{i=1}^{n} p_{\mu i}^{[y]} e^{s_i t}$$

where $p_{\mu i}^{[y]} = c_{\mu 1}p_{1i}^{[x]} + \cdots + c_{\mu n}p_{ni}^{[x]}$ is the (μ, i)-th element of the participation matrix of algebraic variables $\mathbf{P}_y$ as defined in (17).

Appendix B Proof of Proposition 1

We start by introducing parameters a, a^* for the predictor used in step 1) and b, b^*, c, c^* for the solution of fast and slow variables in steps 3) and 4), respectively. These parameters allow the proof to accommodate different combinations of predictor and corrector methods in a unified manner.

For FEM prediction, $a = h_\mathrm{s}$ and $a^* = 0$; for TM prediction, $a = a^* = h_\mathrm{s}/2$; and for BEM prediction, $a = 0$ and $a^* = h_\mathrm{s}$. For the solution of fast and slow variables with TM, $b = b^* = h_\mathrm{f}/2$ and $c = c^* = h_\mathrm{s}/2$; with BEM, $b = c = 0$, $b^* = h_\mathrm{f}$, and $c^* = h_\mathrm{s}$.

Incorporating the parameters a, a^*, b, b^*, c, c^*, (23), (25) and (26) are rewritten as follows:

$$\begin{aligned}
\widetilde{\boldsymbol{x}}_{t+h_\mathrm{s}}^{P} &= \widetilde{\boldsymbol{x}}_t + a\left(\boldsymbol{f}_x\widetilde{\boldsymbol{x}}_t + \boldsymbol{f}_y\widetilde{\boldsymbol{y}}_t\right) + a^*\left(\boldsymbol{f}_x\widetilde{\boldsymbol{x}}_{t+h_\mathrm{s}} + \boldsymbol{f}_y\widetilde{\boldsymbol{y}}_{t+h_\mathrm{s}}\right) \\
\mathbf{0}_{m,1} &= \boldsymbol{g}_x\widetilde{\boldsymbol{x}}_{t+h_\mathrm{s}}^{P} + \boldsymbol{g}_y\widetilde{\boldsymbol{y}}_{t+h_\mathrm{s}}^{P}
\end{aligned} \tag{B.2}$$

$$\begin{aligned}
\widetilde{\boldsymbol{x}}_{\mathrm{f},t+ih_\mathrm{f}} =& \widetilde{\boldsymbol{x}}_{\mathrm{f},t+(i-1)h_\mathrm{f}} + b^*(\boldsymbol{f}_{\mathrm{f},x}\widetilde{\boldsymbol{x}}_{t+ih_\mathrm{f}} + \boldsymbol{f}_{\mathrm{f},y}\widetilde{\boldsymbol{y}}_{t+ih_\mathrm{f}}) \\
&+ b(\boldsymbol{f}_{\mathrm{f},x}\widetilde{\boldsymbol{x}}_{t+(i-1)h_\mathrm{f}} + \boldsymbol{f}_{\mathrm{f},y}\widetilde{\boldsymbol{y}}_{t+(i-1)h_\mathrm{f}}) \\
\mathbf{0}_{m_\mathrm{f},1} =& b^*\left(\boldsymbol{g}_{\mathrm{f},x}\widetilde{\boldsymbol{x}}_{t+ih_\mathrm{f}} + \boldsymbol{g}_{\mathrm{f},y}\widetilde{\boldsymbol{y}}_{t+ih_\mathrm{f}}\right)
\end{aligned} \tag{B.3}$$

$$\begin{aligned}
\widetilde{\boldsymbol{x}}_{\mathrm{s},t+h_\mathrm{s}} &= \widetilde{\boldsymbol{x}}_{\mathrm{s},t} + c^*(\boldsymbol{f}_{\mathrm{s},x}\widetilde{\boldsymbol{x}}_{t+h_\mathrm{s}} + \boldsymbol{f}_{\mathrm{s},y}\widetilde{\boldsymbol{y}}_{t+h_\mathrm{s}}) + c(\boldsymbol{f}_{\mathrm{s},x}\widetilde{\boldsymbol{x}}_t + \boldsymbol{f}_{\mathrm{s},y}\widetilde{\boldsymbol{y}}_t) \\
\mathbf{0}_{m_\mathrm{s},1} &= c^*\left(\boldsymbol{g}_{\mathrm{s},x}\widetilde{\boldsymbol{x}}_{t+h_\mathrm{s}} + \boldsymbol{g}_{\mathrm{s},y}\widetilde{\boldsymbol{y}}_{t+h_\mathrm{s}}\right)
\end{aligned} \tag{B.4}$$

We define:

$$\boldsymbol{f}_x = \begin{bmatrix} \boldsymbol{f}_{\mathrm{ff},x} & \boldsymbol{f}_{\mathrm{fs},x} \\ \boldsymbol{f}_{\mathrm{sf},x} & \boldsymbol{f}_{\mathrm{ss},x} \end{bmatrix} \tag{B.5}$$

where $\boldsymbol{f}_{\mathrm{ff},x} \in \mathbb{R}^{n_\mathrm{f}\times n_\mathrm{f}}$, $\boldsymbol{f}_{\mathrm{fs},x} \in \mathbb{R}^{n_\mathrm{f}\times n_\mathrm{s}}$, $\boldsymbol{f}_{\mathrm{sf},x} \in \mathbb{R}^{n_\mathrm{s}\times n_\mathrm{f}}$ and $\boldsymbol{f}_{\mathrm{ss},x} \in \mathbb{R}^{n_\mathrm{s}\times n_\mathrm{s}}$. Similarly for $\boldsymbol{f}_y$, $\boldsymbol{g}_x$ and $\boldsymbol{g}_y$.

Dividing (B.2) into fast and slow timescales, we have:

$$\begin{aligned}\widetilde{\boldsymbol{x}}^P_{\mathrm{f},t+h_\mathrm{s}} = \widetilde{\boldsymbol{x}}_{\mathrm{f},t} + a\boldsymbol{f}_{\mathrm{ff},x}\widetilde{\boldsymbol{x}}_{\mathrm{f},t} + a\boldsymbol{f}_{\mathrm{fs},x}\widetilde{\boldsymbol{x}}_{\mathrm{s},t} + a\boldsymbol{f}_{\mathrm{ff},y}\widetilde{\boldsymbol{y}}_{\mathrm{f},t} + a\boldsymbol{f}_{\mathrm{fs},y}\widetilde{\boldsymbol{y}}_{\mathrm{s},t} \\ + a^*\boldsymbol{f}_{\mathrm{ff},x}\widetilde{\boldsymbol{x}}_{\mathrm{f},t+h_\mathrm{s}} + a^*\boldsymbol{f}_{\mathrm{fs},x}\widetilde{\boldsymbol{x}}_{\mathrm{s},t+h_\mathrm{s}} + a^*\boldsymbol{f}_{\mathrm{ff},y}\widetilde{\boldsymbol{y}}_{\mathrm{f},t+h_\mathrm{s}} + a^*\boldsymbol{f}_{\mathrm{fs},y}\widetilde{\boldsymbol{y}}_{\mathrm{s},t+h_\mathrm{s}}\end{aligned} \tag{B.6}$$

$$\begin{aligned}\widetilde{\boldsymbol{x}}^P_{\mathrm{s},t+h_\mathrm{s}} = \widetilde{\boldsymbol{x}}_{\mathrm{s},t} + a\boldsymbol{f}_{\mathrm{fs},x}\widetilde{\boldsymbol{x}}_{\mathrm{f},t} + a\boldsymbol{f}_{\mathrm{ss},x}\widetilde{\boldsymbol{x}}_{\mathrm{s},t} + a\boldsymbol{f}_{\mathrm{sf},y}\widetilde{\boldsymbol{y}}_{\mathrm{f},t} + a\boldsymbol{f}_{\mathrm{ss},y}\widetilde{\boldsymbol{y}}_{\mathrm{s},t} \\ + a^*\boldsymbol{f}_{\mathrm{fs},x}\widetilde{\boldsymbol{x}}_{\mathrm{f},t+h_\mathrm{s}} + a^*\boldsymbol{f}_{\mathrm{ss},x}\widetilde{\boldsymbol{x}}_{\mathrm{s},t+h_\mathrm{s}} + a^*\boldsymbol{f}_{\mathrm{fs},y}\widetilde{\boldsymbol{y}}_{\mathrm{f},t+h_\mathrm{s}} + a^*\boldsymbol{f}_{\mathrm{ss},y}\widetilde{\boldsymbol{y}}_{\mathrm{s},t+h_\mathrm{s}}\end{aligned} \tag{B.7}$$

$$\mathbf{0}_{m_\mathrm{f},1} = \boldsymbol{g}_{\mathrm{ff},x}\widetilde{\boldsymbol{x}}^P_{\mathrm{f},t+h_\mathrm{s}} + \boldsymbol{g}_{\mathrm{fs},x}\widetilde{\boldsymbol{x}}^P_{\mathrm{s},t+h_\mathrm{s}} + \boldsymbol{g}_{\mathrm{ff},y}\widetilde{\boldsymbol{y}}^P_{\mathrm{f},t+h_\mathrm{s}} + \boldsymbol{g}_{\mathrm{fs},y}\widetilde{\boldsymbol{y}}^P_{\mathrm{s},t+h_\mathrm{s}} \tag{B.8}$$

$$\mathbf{0}_{m_\mathrm{s},1} = \boldsymbol{g}_{\mathrm{sf},x}\widetilde{\boldsymbol{x}}^P_{\mathrm{f},t+h_\mathrm{s}} + \boldsymbol{g}_{\mathrm{ss},x}\widetilde{\boldsymbol{x}}^P_{\mathrm{s},t+h_\mathrm{s}} + \boldsymbol{g}_{\mathrm{sf},y}\widetilde{\boldsymbol{y}}^P_{\mathrm{f},t+h_\mathrm{s}} + \boldsymbol{g}_{\mathrm{ss},y}\widetilde{\boldsymbol{y}}^P_{\mathrm{s},t+h_\mathrm{s}} \tag{B.9}$$

From (B.8), we have:

$$\widetilde{\boldsymbol{y}}^P_{\mathrm{f},t+h_\mathrm{s}} = -\boldsymbol{g}^{-1}_{\mathrm{ff},y}(\boldsymbol{g}_{\mathrm{ff},x}\widetilde{\boldsymbol{x}}^P_{\mathrm{f},t+h_\mathrm{s}} + \boldsymbol{g}_{\mathrm{fs},x}\widetilde{\boldsymbol{x}}^P_{\mathrm{s},t+h_\mathrm{s}} + \boldsymbol{g}_{\mathrm{fs},y}\widetilde{\boldsymbol{y}}^P_{\mathrm{s},t+h_\mathrm{s}}) \tag{B.10}$$

Note that the invertibility of $\mathbf{g}_{\mathrm{ff},y}$ is used here to facilitate derivation; however, it is not strictly required provided that a sparse matrix formulation is adopted, similarly e.g., to [27].

Based on (B.6)-(B.10), we get the expression of $\widetilde{\boldsymbol{y}}^P_{\mathrm{s},t+h_\mathrm{s}}$:

$$\begin{aligned}\widetilde{\boldsymbol{y}}^P_{\mathrm{s},t+h_\mathrm{s}} = (-\mathbf{H}_3{}^{-1}\mathbf{H}_1 + \mathbf{M}_1)\widetilde{\boldsymbol{x}}_{\mathrm{f},t} + (-\mathbf{H}_3{}^{-1}\mathbf{H}_1 + \mathbf{M}_2)\widetilde{\boldsymbol{x}}_{\mathrm{s},t} \\ + \mathbf{M}_3\widetilde{\boldsymbol{y}}_{\mathrm{f},t} + \mathbf{M}_4\widetilde{\boldsymbol{y}}_{\mathrm{s},t} + \mathbf{M}^*_1\widetilde{\boldsymbol{x}}_{\mathrm{f},t+h_\mathrm{s}} + \mathbf{M}^*_2\widetilde{\boldsymbol{x}}_{\mathrm{s},t+h_\mathrm{s}} \\ + \mathbf{M}^*_3\widetilde{\boldsymbol{y}}_{\mathrm{f},t+h_\mathrm{s}} + \mathbf{M}^*_4\widetilde{\boldsymbol{y}}_{\mathrm{s},t+h_\mathrm{s}}\end{aligned} \tag{B.11}$$

where

$$\begin{aligned}\mathbf{M}_1 &= -a\mathbf{H}_3{}^{-1}\mathbf{H}_1\boldsymbol{f}_{\mathrm{ff},x} - a\mathbf{H}_3{}^{-1}\mathbf{H}_2\boldsymbol{f}_{\mathrm{sf},x} \\ \mathbf{M}_2 &= -a\mathbf{H}_3{}^{-1}\mathbf{H}_1\boldsymbol{f}_{\mathrm{fs},x} - a\mathbf{H}_3{}^{-1}\mathbf{H}_2\boldsymbol{f}_{\mathrm{ss},x} \\ \mathbf{M}_3 &= -a\mathbf{H}_3{}^{-1}\mathbf{H}_1\boldsymbol{f}_{\mathrm{ff},y} - a\mathbf{H}_3{}^{-1}\mathbf{H}_2\boldsymbol{f}_{\mathrm{sf},y} \\ \mathbf{M}_4 &= -a\mathbf{H}_3{}^{-1}\mathbf{H}_1\boldsymbol{f}_{\mathrm{fs},y} - a\mathbf{H}_3{}^{-1}\mathbf{H}_2\boldsymbol{f}_{\mathrm{ss},y}\end{aligned}$$

Replace a in $\mathbf{M}_1$ to $\mathbf{M}_4$ as a^* for $\mathbf{M}^*_1$ to $\mathbf{M}^*_4$. For $i = 1$, combining (24), (B.3) and (B.11) establishes the relationship between $\mathbf{x}_{t+ih_\mathrm{f}}$, $\mathbf{x}_{t+(i-1)h_\mathrm{f}}$ and $\mathbf{x}_{t+h_\mathrm{s}}$ over the interval $[t(i-1)h_\mathrm{f}, t+ih_\mathrm{f}]$ for the multirate method ($i \leq r-1$):

$$-\mathbf{C}_i\mathbf{x}_{t+h_\mathrm{s}} + \mathbf{Z}_i\mathbf{x}_{t+ih_\mathrm{f}} = \mathbf{B}_i\mathbf{x}_{t+(i-1)h_\mathrm{f}} \tag{B.12}$$

with

$$\mathbf{C}_i = \frac{i}{r}\begin{bmatrix} \mathbf{0}_{n_\mathrm{f},n_\mathrm{f}} & \mathbf{0}_{n_\mathrm{f},n_\mathrm{s}} & \mathbf{0}_{n_\mathrm{f},m_\mathrm{f}} & \mathbf{0}_{n_\mathrm{f},m_\mathrm{s}} \\ a^*\boldsymbol{f}_{\mathrm{sf},x} & a^*\boldsymbol{f}_{\mathrm{ss},x} & a^*\boldsymbol{f}_{\mathrm{sf},y} & a^*\boldsymbol{f}_{\mathrm{ss},y} \\ \mathbf{0}_{m_\mathrm{f},n_\mathrm{f}} & \mathbf{0}_{m_\mathrm{f},n_\mathrm{s}} & \mathbf{0}_{m_\mathrm{f},m_\mathrm{f}} & \mathbf{0}_{m_\mathrm{f},m_\mathrm{s}} \\ \mathbf{M}_1^* & \mathbf{M}_2^* & \mathbf{M}_3^* & \mathbf{M}_4^* \end{bmatrix}$$

$$\mathbf{Z}_i = \boldsymbol{I}_{n_\mathrm{f}} \oplus \mathbf{0}_{n_\mathrm{s}+m} + (-b\boldsymbol{I}_{n_\mathrm{f}}) \oplus \boldsymbol{I}_{n_\mathrm{s}} \oplus (-b\boldsymbol{I}_{m_\mathrm{f}}) \oplus \boldsymbol{I}_{m_\mathrm{s}} \times \begin{bmatrix} \boldsymbol{f}_{\mathrm{ff},x} & \boldsymbol{f}_{\mathrm{fs},x} & \boldsymbol{f}_{\mathrm{ff},y} & \boldsymbol{f}_{\mathrm{fs},y} \\ \mathbf{0}_{n_\mathrm{s},n_\mathrm{f}} & \boldsymbol{I}_{n_\mathrm{s}} & \mathbf{0}_{n_\mathrm{s},m_\mathrm{f}} & \mathbf{0}_{n_\mathrm{s},m_\mathrm{s}} \\ \boldsymbol{g}_{\mathrm{ff},x} & \boldsymbol{g}_{\mathrm{fs},x} & \boldsymbol{g}_{\mathrm{ff},y} & \boldsymbol{g}_{\mathrm{fs},y} \\ \mathbf{0}_{m_\mathrm{s},n_\mathrm{f}} & \mathbf{0}_{m_\mathrm{s},n_\mathrm{s}} & \mathbf{0}_{m_\mathrm{s},m_\mathrm{f}} & \boldsymbol{I}_{m_\mathrm{s}} \end{bmatrix}$$

$$\mathbf{B}_i = \boldsymbol{I}_{n_\mathrm{f}} \oplus \mathbf{0}_{n_\mathrm{s}+m} + \mathbf{C}_i + (b^*\boldsymbol{I}_{n_\mathrm{f}}) \oplus \boldsymbol{I}_{n_\mathrm{s}} \oplus (b^*\boldsymbol{I}_{m_\mathrm{f}}) \oplus (\frac{i}{r})\boldsymbol{I}_{m_\mathrm{s}} \times \begin{bmatrix} \boldsymbol{f}_{\mathrm{ff},x} & \boldsymbol{f}_{\mathrm{fs},x} & \boldsymbol{f}_{\mathrm{ff},y} & \boldsymbol{f}_{\mathrm{fs},y} \\ a\boldsymbol{f}_{\mathrm{sf},x} & \boldsymbol{I}_{n_\mathrm{s}} + a\boldsymbol{f}_{\mathrm{ss},x} & a\boldsymbol{f}_{\mathrm{sf},y} & a\boldsymbol{f}_{\mathrm{ss},y} \\ \boldsymbol{g}_{\mathrm{ff},x} & \boldsymbol{g}_{\mathrm{fs},x} & \boldsymbol{g}_{\mathrm{ff},y} & \boldsymbol{g}_{\mathrm{fs},y} \\ -\mathbf{H}_3{}^{-1}\mathbf{H}_1 + \mathbf{M}_1 & -\mathbf{H}_3{}^{-1}\mathbf{H}_2 + \mathbf{M}_2 & \mathbf{M}_3 & (\frac{r}{i} - 1)\boldsymbol{I}_{m_\mathrm{s}} + \mathbf{M}_4 \end{bmatrix}$$

At $i = r$, the slow variables are integrated with the TM, and the relationship between $\mathbf{x}_{t+(r-1)h_\mathrm{f}}$, $\mathbf{x}_t$ and $\mathbf{x}_{t+h_\mathrm{s}}$ over the interval $[t + (r-1)h_\mathrm{f}, t + h_\mathrm{s}]$ for the multirate method:

$$\mathbf{Z}_r \mathbf{x}_{t+h_\mathrm{s}} = \mathbf{B}_r \mathbf{x}_{t+(r-1)h_\mathrm{f}} + \mathbf{C}_r \mathbf{x}_t \tag{B.13}$$

with

$$\mathbf{Z}_r = \mathbf{E} - (b\boldsymbol{I}_{n_\mathrm{f}} \oplus c\boldsymbol{I}_{n_\mathrm{s}} \oplus b\boldsymbol{I}_{m_\mathrm{f}} \oplus c\boldsymbol{I}_{m_\mathrm{s}})\mathbf{A}$$

$$\mathbf{C}_r = \mathbf{0}_{n_\mathrm{f}} \oplus \boldsymbol{I}_{n_\mathrm{s}} \oplus \mathbf{0}_m + \boldsymbol{I}_{n_\mathrm{f}} \oplus c^*\boldsymbol{I}_{n_\mathrm{s}} \oplus \boldsymbol{I}_{m_\mathrm{f}} \oplus c^*\boldsymbol{I}_{m_\mathrm{s}} \times \begin{bmatrix} \mathbf{0}_{n_\mathrm{f}} & \mathbf{0}_{n_\mathrm{f},n_\mathrm{s}} & \mathbf{0}_{n_\mathrm{f},m_\mathrm{f}} & \mathbf{0}_{n_\mathrm{f},m_\mathrm{s}} \\ \boldsymbol{f}_{\mathrm{sf},x} & \boldsymbol{f}_{\mathrm{ss},x} & \boldsymbol{f}_{\mathrm{sf},y} & \boldsymbol{f}_{\mathrm{ss},y} \\ \mathbf{0}_{m_\mathrm{f},n_\mathrm{f}} & \mathbf{0}_{m_\mathrm{f},n_\mathrm{s}} & \mathbf{0}_{m_\mathrm{f}} & \mathbf{0}_{m_\mathrm{f},m_\mathrm{s}} \\ \boldsymbol{g}_{\mathrm{sf},x} & \boldsymbol{g}_{\mathrm{ss},x} & \boldsymbol{g}_{\mathrm{sf},y} & \boldsymbol{g}_{\mathrm{ss},y} \end{bmatrix}$$

$$\mathbf{B}_r = \boldsymbol{I}_{n_\mathrm{f}} \oplus \mathbf{0}_{n_\mathrm{s}+m} + (b^*\boldsymbol{I}_{n_\mathrm{f}}) \oplus \boldsymbol{I}_{n_\mathrm{s}} \oplus (b^*\boldsymbol{I}_{m_\mathrm{f}}) \oplus \boldsymbol{I}_{m_\mathrm{s}} \times \begin{bmatrix} \boldsymbol{f}_{\mathrm{ff},x} & \boldsymbol{f}_{\mathrm{fs},x} & \boldsymbol{f}_{\mathrm{ff},y} & \boldsymbol{f}_{\mathrm{fs},y} \\ \mathbf{0}_{n_\mathrm{s},n_\mathrm{f}} & \mathbf{0}_{n_\mathrm{s}} & \mathbf{0}_{n_\mathrm{s},m_\mathrm{f}} & \mathbf{0}_{n_\mathrm{s},m_\mathrm{s}} \\ \boldsymbol{g}_{\mathrm{ff},x} & \boldsymbol{g}_{\mathrm{fs},x} & \boldsymbol{g}_{\mathrm{ff},y} & \boldsymbol{g}_{\mathrm{fs},y} \\ \mathbf{0}_{m_\mathrm{s},n_\mathrm{f}} & \mathbf{0}_{m_\mathrm{s},n_\mathrm{s}} & \mathbf{0}_{m_\mathrm{s},m_\mathrm{f}} & \mathbf{0}_{m_\mathrm{s}} \end{bmatrix}$$

Finally, we arrive to a system in the form of (18), where:

$$\mathbf{F}_r = \begin{bmatrix} \mathbf{Z}_r & & \\ \vdots & \ddots & \\ -\mathbf{C}_1 & & \mathbf{Z}_1 \end{bmatrix}, \quad \mathbf{G}_r = \begin{bmatrix} \mathbf{B}_r & & \mathbf{C}_r \\ & \ddots & \\ & & \mathbf{B}_1 \end{bmatrix}$$

References

[1] S. D. Pekarek, O. Wasynczuk, E. A. Walters, J. V. Jatskevich, C. E. Lucas, N. Wu, and P. T. Lamm, "An efficient multirate simulation technique for power-electronic-based systems," *IEEE Transactions on Power Systems*, vol. 19, no. 1, pp. 399–409, 2004.

[2] Q. Li, D. Wang, X. Liang, Y. Qin, Y. Zhang, and C. Ma, "An iteratively-nested modeling method for stability analysis of the multirate power system," *IEEE Transactions on Industrial Informatics*, 2023.

[3] J. Chen and M. L. Crow, "A variable partitioning strategy for the multirate method in power systems," *IEEE Transactions on Power Systems*, vol. 23, no. 2, pp. 259–266, 2008.

[4] M. Crow and J. G. Chen, "The multirate method for simulation of power system dynamics," *IEEE Transactions on Power Systems*, vol. 9, no. 3, pp. 1684–1690, 1994.

[5] T. Kato, K. Inoue, T. Fukutani, and Y. Kanda, "Multirate analysis method for a power electronic system by circuit partitioning," *IEEE Transactions on Power Electronics*, vol. 24, no. 12, pp. 2791–2802, 2009.

[6] Y. Huang, Q. Sun, Y. Li, W. Gao, and D. W. Gao, "A multi-rate dynamic energy flow analysis method for integrated electricity-gas-heat system with different time-scale," *IEEE Transactions on Power Delivery*, vol. 38, no. 1, pp. 231–243, 2023.

[7] A. Peiret, F. González, J. Kövecses, and M. Teichmann, "Multibody system dynamics interface modelling for stable multirate co-simulation of multiphysics systems," *Mechanism and Machine Theory*, vol. 127, pp. 52–72, 2018.

[8] G. Lauss and K. Strunz, "Multirate partitioning interface for enhanced stability of power hardware-in-the-loop real-time simulation," *IEEE Transactions on Industrial Electronics*, vol. 66, no. 1, pp. 595–605, 2019.

[9] M. Crow and J. G. Chen, "The multirate simulation of FACTS devices in power system dynamics," in *Proceedings of Power Industry Computer Applications Conference*. IEEE, 1995, pp. 290–296.

[10] V. Savcenco and B. Haut, "Construction and analysis of an automatic multirate time domain simulation method for large power systems," *Electric power systems research*, vol. 107, pp. 28–35, 2014.

[11] G. Tzounas, I. Dassios, and F. Milano, "Modal participation factors of algebraic variables," *IEEE Transactions on Power Systems*, vol. 35, no. 1, pp. 742–750, 2019.

[12] H. Lin, S. S. Veda, S. S. Shukla, L. Mili, and J. Thorp, "GECO: Global event-driven co-simulation framework for interconnected power system and communication network," *IEEE Transactions on Smart Grid*, vol. 3, no. 3, pp. 1444–1456, 2012.

[13] R. Venkatraman, S. K. Khaitan, and V. Ajjarapu, "Dynamic co-simulation methods for combined transmission-distribution system with integration time step impact on convergence," *IEEE Transactions on Power Systems*, vol. 34, no. 2, pp. 1171–1181, 2018.

[14] D. Shu, X. Xie, Q. Jiang, G. Guo, and K. Wang, "A multirate EMT co-simulation of large AC and MMC-based MTDC systems," *IEEE Transactions on Power Systems*, vol. 33, no. 2, pp. 1252–1263, 2017.

[15] C. W. Gear, "Multirate methods for ordinary differential equations," Illinois Univ., Urbana (USA). Dept. of Computer Science, Tech. Rep., 1974.

[16] G. Tzounas, I. Dassios, and F. Milano, "Small-signal stability analysis of numerical integration methods," *IEEE Transactions on Power Systems*, vol. 37, no. 6, pp. 4796–4806, 2022.

[17] G. Tzounas, I. Dassios, and F. Milano, "Small-signal stability analysis of implicit integration methods for power systems with delays," *Electric Power Systems Research*, vol. 211, p. 108266, 2022.

[18] A. Bouterakos and G. Tzounas, "Stability of the Theta method for systems with multiple time-delayed variables," *submitted to the IEEE Transactions on Power Systems*, 2025, under review. Available at arxiv.org/abs/2409.04399.

[19] C. Tajoli, G. Tzounas, and G. Hug, "Mode-shape deformation of power system DAEs by time-domain integration methods," in *2023 IEEE Belgrade PowerTech*. IEEE, 2023, pp. 1–6.

[20] P. Kundur, *Power System Stability and Control*. New York: Mc-Grall Hill, 1994.

[21] F. Milano, M. Liu, M. A. Murad, G. M. Jónsdóttir, G. Tzounas, M. Adeen, Á. Ortega, and I. Dassios, "Power system modelling as stochastic functional hybrid differential-algebraic equations," *IET Smart Grid*, vol. 5, no. 5, pp. 309–331, 2022.

[22] F. Milano, I. Dassios, M. Liu, and G. Tzounas, *Eigenvalue Problems in Power Systems*. CRC Press, 2020.

[23] D. Moutevelis, G. Tzounas, J. Roldán-Pérez, and F. Milano, "Modal propagation analysis with participation factors of complex frequency variables," *Electric Power Systems Research*, vol. 230, p. 110295, 2024.

[24] P. W. Sauer, M. A. Pai, and J. H. Chow, *Power system dynamics and stability: with synchrophasor measurement and power system toolbox*. John Wiley & Sons, 2017.

[25] F. Milano, "A Python-based software tool for power system analysis," in *2013 IEEE Power & Energy Society General Meeting*. IEEE, 2013, pp. 1–5.

[26] E. Anderson, Z. Bai, C. Bischof, J. Demmel, J. Dongarra, J. DuCroz, A. Greenbaum, S. Hammarling, A. McKenney, and D. Sorensen, *LAPACK: A Portable Linear Algebra Library for High-Performance Computers*, 1990.

[27] G. Tzounas and G. Hug, "Unified numerical stability and accuracy analysis of the partitioned-solution approach," *IEEE Transactions on Power Systems*, vol. 39, no. 2, pp. 3141–3152, 2023.